Nanoscale

REVIEW

View Article Online
View Journal | View Issue

Cite this: *Nanoscale*, 2024, **16**, 21279

Recent advances in tungsten oxide-based chromogenic materials: photochromism, electrochromism, and gasochromism

Yaqi Zhang,[a,b] Yilin Ding,[a] Fan Lan,[a] Wenjing Zhang,[a] Jingfa Li *[b] and Rufan Zhang *[a]

As n-type and wide-bandgap semiconductor materials which are widely found in nature, tungsten oxides (WO_x) have attracted extensive attention because of their rich phase structures and unique sub-stoichiometric properties. Tungsten oxides have a good chromogenic response to optical, electrical, and gaseous stimuli, in which their phase changes with the change of temperature and ionic embeddedness, accompanied by significant changes in their optical properties. In addition, due to the presence of oxygen defects, the conductivity and adsorption capacity of tungsten oxides for surface substances are enhanced. These properties endow tungsten oxides with promising application potential in the optical and electronic device areas. This paper reviews the structural and optoelectrical properties of tungsten oxide-based chromogenic materials. Then we focus on the working mechanisms, performance indexes, and preparation methods of tungsten oxides in the field of intelligent chromogenic technology, including photochromism, electrochromism, and gasochromism of tungsten oxide-based chromogenic materials. Finally, a conclusion and outlook are provided, which may help to further advance the application of tungsten oxides in the field of smart chromogenic changes.

Received 14th September 2024,
Accepted 17th October 2024

DOI: 10.1039/d4nr03781b

rsc.li/nanoscale

1. Introduction

In recent years, the fast-growing global energy consumption and carbon dioxide emission have posed serious challenges to the sustainable development of human society. Therefore, it is of significant importance to develop green, clean, and renewable energy technologies. Tremendous efforts have been made in recent years on solar cells,[9,10] fuel cells,[14] photocatalytic

[a]*Beijing Key Laboratory of Green Chemical Reaction Engineering and Technology, Department of Chemical Engineering, Tsinghua University, Beijing 100084, China. E-mail: zhangrufan@tsinghua.edu.cn*
[b]*Jiangsu Key Laboratory of New Energy Devices & Interface Science, School of Chemistry and Materials Science, Nanjing University of Information Science and Technology, Nanjing 210044, China. E-mail: aplijf@nuist.edu.cn*

Yaqi Zhang

Yaqi Zhang received her B.S. degree from Southwest University in 2021. Currently, she is pursuing her M.S. degree in the School of Chemistry and Materials, Nanjing University of Information Engineering and is an exchange student at the Department of Chemical Engineering, Tsinghua University, under the supervision of Prof. Jingfa Li and Prof. Rufan Zhang. Her main research interests include electrochromic materials and devices.

Yilin Ding

Yilin Ding received her PhD degree in Condensed Matter Physics from Beihang University, China (2023), under the guidance of Prof. Xungang Diao. Currently, she is conducting her postdoctoral work in the Department of Chemical Engineering, Tsinghua University. Her main research focuses on electrochromic materials and devices.

materials,[19] and photothermal management materials.[20,21] Among the most commonly used photothermal management materials, intelligent chromogenic materials have attracted wide attention because of their advantages in smart windows, building envelope materials and infrared camouflage.[22–25] The optical properties of intelligent chromogenic materials can be largely changed under external stimuli such as light, electricity, heat, pressure, *etc.* As abundant semiconductor materials found in nature, tungsten oxides (WO_x) have a chromogenic response to a wide range of external stimuli such as light, electricity, and gas, which are therefore considered as among the most popular inorganic intelligent chromogenic materials.

Tungsten oxides have various phase structures, which can be converted between each other with changes in temperature and the extent of ionic embedding, accompanied by significant changes in their optical properties, such as visible and infrared light transmittance, absorbance, reflectance, *etc.* Therefore, tungsten oxide materials have photochromic, electrochromic, gasochromic and thermochromic properties. A perfect WO_3 crystal is a cubic crystal composed of [WO_6] octahedra in a co-vertex mode and is the same as the ReO_3-type chalcogenide structure, which endows WO_3 with an excellent charge storage and transfer capability. In addition, WO_{xx} has unique sub-stoichiometric properties. Due to the presence of different degrees of oxygen defects, its electrical conductivity, adsorption capacity for surface substances, *etc.* are enhanced to different extents. In recent years, the complex multivalent properties and multi-defect structure of WO_x have shown great potential for applications in lithium batteries, supercapacitors, gas sensors, and smart windows (Fig. 1).[29–33]

Herein, we briefly review the structural and sub-stoichiometric properties of WO_x materials and introduce the influence of these properties on their optoelectrical performance. Then we discuss the working mechanism of WO_x materials in intelligent chromogenic technology, including photochromism, electrochromism and gasochromism, evaluation indicators and the methods of performance enhancement.

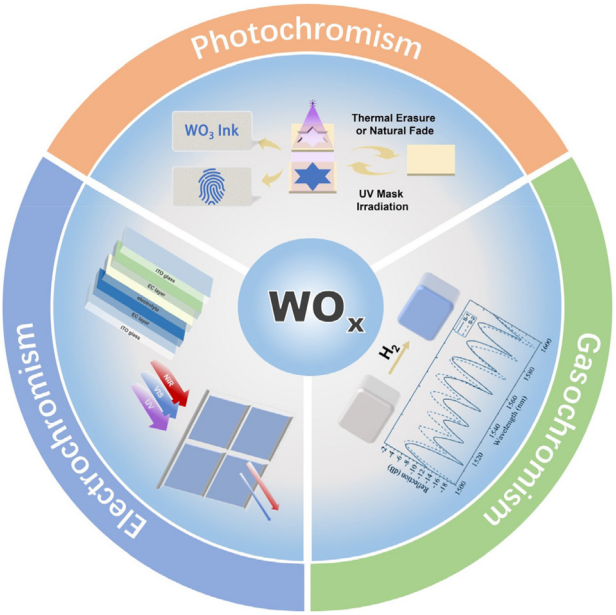

Fig. 1 Applications of WO_x in photochromic, electrochromic, and gasochromic materials and devices.

2. Fundamental properties of WO_x

Materials are intricately linked between their structures and properties. The WO_x family is a series of materials with diverse structures and complex chemical states, a feature that makes the variation of its optical and electrical properties of great interest.

2.1 Crystallography and sub-chemometrics

As a common member of the WO_x family, the WO_3 crystal is a cubic crystal composed of [WO_6] octahedra in a co-vertex manner, which is shown in Fig. 2a. In other WO_3 crystal forms, it can be seen as an assembly of structural units

Jingfa Li

Jingfa Li received his PhD degree from the University of Science and Technology of China in 2012. After that, he moved overseas to the University of Wollongong in Australia and the National University of Singapore to pursue his postdoctoral research. He joined in Nanjing University of Information Science and Technology as a full-time professor in 2016. His research interests mainly focus on the design and synthesis of novel micro-/nanostructured materials for energy conversion and storage devices.

Rufan Zhang

Rufan Zhang recieved his PhD degree from Tsinghua University in 2014. After that, he worked as a postdoctoral researcher in the Department of Materials at Stanford University. He joined Tsinghua University in 2018 and was appointed as an associate professor in the Department of Chemical Engineering at Tsinghua University in 2019. His research interests mainly focus on carbon nanotubes and functional fibers, electrochromic materials and devices, structural chromogenic materials, radiation-cooled materials, and zinc–air battery catalysts.

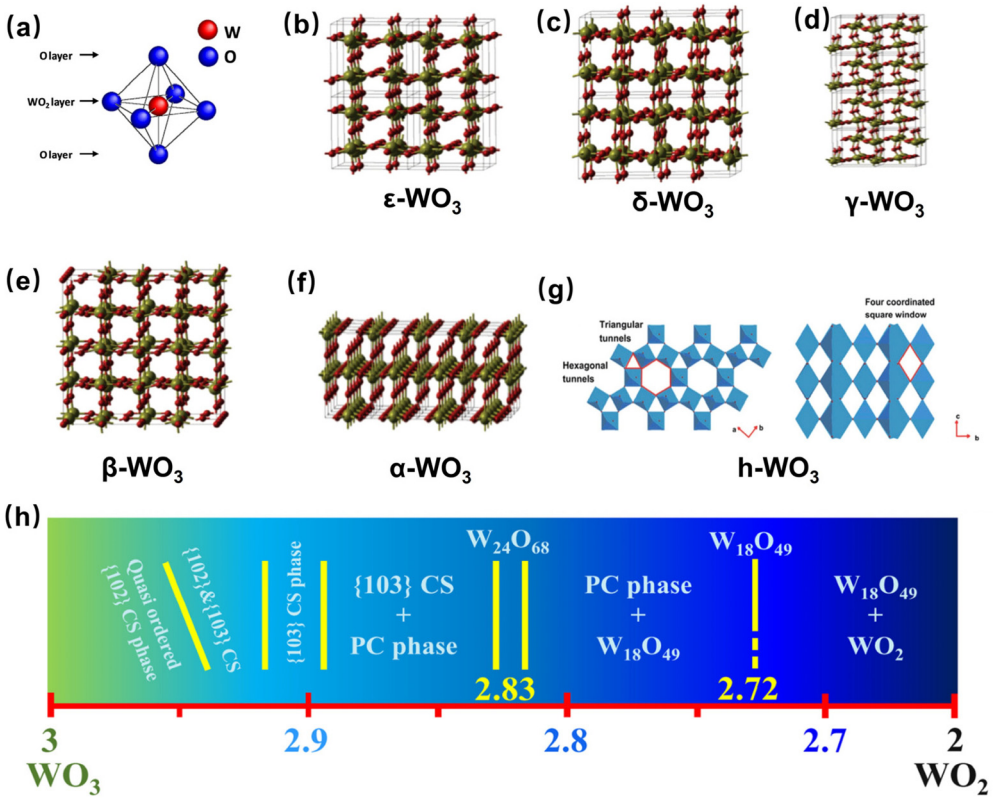

Fig. 2 (a) Ideal WO_3 crystal. (b) Monoclinic WO_3. (c) Triclinic WO_3. (d) Monoclinic WO_3 (17–330 °C). (e) Orthorhombic WO_3. (f) Tetragonal WO_3. (g) Hexagonal WO_3. Reproduced with permission.[4] Copyright 2019, John Wiley and Sons. (h) Sub-stoichiometric WO_{3-x}. Reproduced with permission.[12] Copyright 2021, Springer Nature.

obtained by rotating or twisting on the basis of an ideal WO_3 crystal structure. As the temperature increases, WO_3 undergoes a phase transition, which varies sequentially from ε-WO_3 (monoclinic phase, below −43 °C) to δ-WO_3 (triclinic phase, −43–17 °C), γ-WO_3 (monoclinic phase, 17–330 °C), β-WO_3 (orthorhombic phase, 330–740 °C), and α-WO_3 (tetragonal phase, above 740 °C) (Fig. 2b–f).[4,34] Among various types of WO_3, γ-WO_3 is the most common stable phase at room temperature. Besides the above-mentioned crystal types, h-WO_3 (hexagonal phase) is also a relatively stable crystal type of WO_3 (Fig. 2g).[4] However, it cannot be obtained from other crystalline structures by heat treatment but can only be prepared by dehydration of WO_3 with water of crystallization. Such specific preparation conditions result in the presence of many hexagonal and triangular pores in h-WO_3, which facilitates the transport of ions inside the structure and also provides active space for redox reactions. Compared with crystalline tungsten oxides, amorphous tungsten oxides have disordered bond lengths and bond angles, and there are a large number of dangling bonds and various structural distortions and defects in their distorted structures with a more active electronic structure.[35] Higher atomic disorder and interstitial spacing of amorphous phase tungsten oxide can serve as a fast channel for ion diffusion, exhibiting excellent properties and performance of tungsten oxides-based electrochromic devices.[36] In general, amorphous tungsten oxides have enhanced optical modulation and coloring efficiency over bulk crystalline films due to their relatively loose structure, yet their stability is limited.

Based on the content of oxygen vacancies in the lattice, WO_x is classified as stoichiometric WO_x and sub-stoichiometric WO_x. In 1989, Glember and Saurr first found the sub-stoichiometric properties of WO_x.[37,92] Since then, a large number of WO_x materials with sub-stoichiometric ratios have been continuously reported, in which the value of x is between 2 and 3, which represents the concentration of oxygen vacancies. Thus, a series of sub-stoichiometric WO_x materials (including $W_{32}O_{84}$, W_3O_8, $W_{18}O_{49}$, $W_{17}O_{47}$, W_5O_{14}, $W_{20}O_{58}$, *etc.*) exist between the two stable tungsten oxides, WO_3 and WO_2 (Fig. 2h).[12] The crystal structure of sub-stoichiometric WO_x is similar to that of stoichiometric WO_3, also composed of co-rimmed [WO_6] octahedra, with the difference that the ordered oxygen defect surface acts as its crystal shear (CS) surface to split it.[38] $WO_{2.87}$ and higher concentrations of oxygen vacancies in WO_x result in the formation of pentagonal columns (PCs), leading to the appearance of new crystalline phases.[12] Taking the advantage of the structural features of the [WO_6] octahedral edges, the WO_x lattice can withstand a considerable degree of oxygen deficiency, and part of W^{6+} atoms are reduced to W^{5+}. The absence of lattice oxygen atoms affects the energy gap and free electron density of WO_x. With

the increase of oxygen vacancy concentration, the metallic properties of WO_x are revealed. Therefore, diverse and interesting physicochemical properties can be tapped by simply modulating the stoichiometric ratio of WO_x.

2.2 Optical and electrical properties

WO_x is an n-type and wide-bandgap semiconductor material with an indirect bandgap between the valence and conduction bands, where the valence band consists mainly of O 2p orbitals and the conduction band consists mainly of W 5d orbitals.[37] W 5d orbital occupancy is strongly correlated with lattice distortion, thus the change in crystal phase has a significant effect on the band gap of WO_x. The bandgap of bulk phase γ-WO_3 is usually in the range of 2.6–2.8 eV. The bandgap varies with the degree of distortion of the crystal structure, therefore amorphous WO_x with large lattice distortion has a wide bandgap of 3.4 eV. Apart from the crystalline phase structure, the size of the WO_x material also affects its band gap. Due to the quantum confinement effect, when the size of WO_x is close to or smaller than its exciton Bohr radius (3 nm), its bandgap becomes wider as the particle size decreases. In contrast, when the crystal size is larger than the exciton Bohr radius, the effect of size on the bandgap diminishes.[39]

Standard stoichiometric WO_3 powder is yellow, while sub-stoichiometric WO_x is variable in color. For instance, $WO_{2.9}$ is bluish-purple, $WO_{2.72}$ is purplish-red, and WO_2 is brown. The light absorption range of WO_x covers the entire solar spectrum, *i.e.*, the ultraviolet, visible, and near-infrared bands, and the whole process involves electron interbond leaps, polariton leaps, and plasmon resonance (LSPR).[40–42] Absorption in the visible region may be related to the level of oxygen defects, a process that can be elucidated in terms of the polariton jump mechanism. The injected electrons are first trapped by the W 5d orbitals, and the lattice around them undergoes polarization to produce polaritons. Incident photons can induce mutual leaps of polaritons from two neighboring W sites, which is thought to be the reason for the blue color of WO_x materials when stimulated by light, gases, and electric fields.[37]

In recent years, near-infrared absorption of sub-stoichiometric WO_x has also received extensive attention. Sub-stoichiometric WO_x has oxygen vacancies that increase its carrier density. At higher concentrations of oxygen vacancies, the absorption of WO_x in the near-infrared (NIR) band is greatly increased, which is usually attributed to the generation of the LSPR effect.[43,44] LSPR is usually found in noble metal nanoparticles, which absorb photon energy strongly when the incident photon frequency matches the overall vibrational frequency of the carriers, which results in a strong resonance absorption peak in the spectrum. Sub-stoichiometric WO_x is distinguished from other semiconductor oxides due to its rather high carrier density, which is also necessary for the strong LSPR effect.[8,45–48] The tunable plasmon resonance of sub-stoichiometric WO_x gives it a strong absorption in the near-infrared region, and therefore has a great potential for application in the field of building energy efficiency.

3. Photothermal management applications

Owing to its unique physicochemical properties, WO_x offers great potential for its application in optical and electrical fields. This section focuses on the working mechanism, performance indexes, and preparation methods of WO_x in intelligent chromogenic technologies, including photochromism, electrochromism, and gasochromism.

3.1 Photochromism

Photochromism is one of important branch of photochemical and photophysical applications which is a reversible process triggered by light absorption and other external stimuli (*e.g.*, light avoidance, thermal stimuli, *etc.*). As shown in Fig. 3a, a chemical reaction occurs when A is irradiated with light to produce product B. B is then able to be reconverted to A after overcoming an energy barrier or a photothermal stimulus, with a distinct difference in its absorption spectrum and a change in color.[1] Photostimulation has the advantages of being clean and contactless, and can be adjusted remotely and precisely (wavelength, intensity, coverage area, duration, *etc.*). Therefore, photochromic materials have a promising application in the fields of data storage,[49,50] information displays,[11] sensors,[26] erasable rewritable paper,[5] and smart windows.[51–53]

WO_x, as the most representative inorganic photochromic material, has received much attention. Although the photochromism of WO_x has been studied for several decades, the mechanism of photochromism is still not well defined. Researchers have proposed many different models to explain the photochromic phenomenon on the basis of their respective experiments. Here, we give a brief overview of the photochromic mechanism of WO_3. Under UV irradiation, WO_3 produces photogenerated electrons and holes (eqn (1)). The photogenerated holes decompose the adsorbed water of the material, thereby generating protons, which participate in water decomposition together with the photogenerated electrons (eqn (2)). The photogenerated electrons and protons then reduce some of the W^{6+} ions in the WO_3 to W^{5+}, forming a blue tungsten bronze at the same time (eqn (3)). The tungsten bronze is oxidized by oxygen in the air (eqn (4)), a process known as photochromic bleaching.

$$WO_3 + h\nu \rightarrow WO_3^* + e^- + h^+ \quad (1)$$

$$H_2O + 2h^+ \rightarrow 2H^+ + O \quad (2)$$

$$WO_3 + xH^+ + xe^- \rightarrow H_xW_{1-x}{}^{6+}W_x{}^{5+}O_3 \quad (3)$$

$$H_xW_{1-x}{}^{6+}W_x{}^{5+}O_3 + \frac{x}{4}O_2 \rightarrow WO_3 + \frac{x}{2}H_2O \quad (4)$$

Excitation wavelength, coloring time, bleaching conditions, bleaching time, and the degree of color changes are key parameters for evaluating photochromic performance. The excitation wavelength is the maximum absorption wavelength that can trigger the photochromic behavior, and a larger excitation

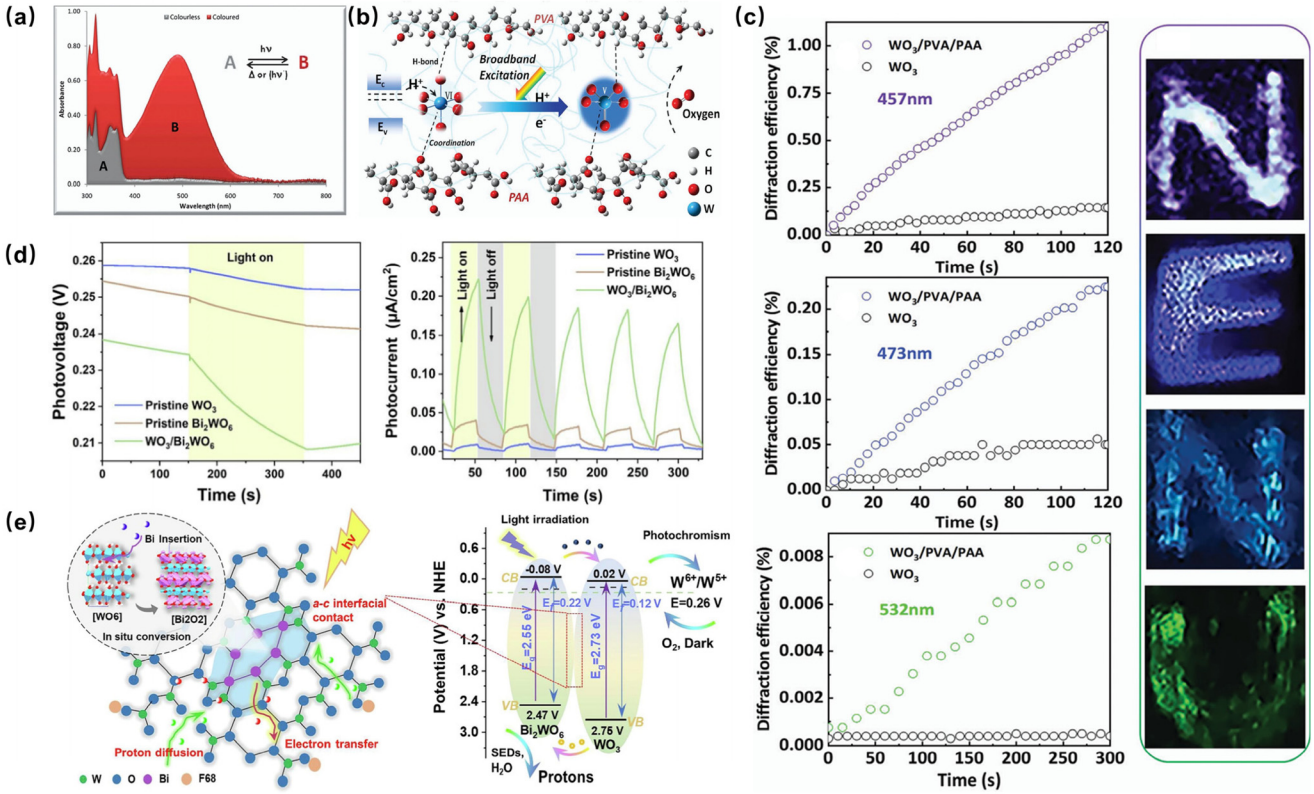

Fig. 3 (a) Photochromic process. Reproduced with permission.[1] Copyright 2011, Royal Society of Chemistry. (b) Illustration of the photochemical reaction mechanism in the WO_3/PVA/PAA hybrid system. (c) Time evolution and color holographic reconstruction of the first-order diffraction efficiency in the recorded configurations at 457 nm, 473 nm and 532 nm for WO_3 and WO_3/PVA/PAA films. Reproduced with permission.[13] Copyright 2022, Royal Society of Chemistry. (d) Transient photovoltaic and photocurrent responses of pristine WO_3, pristine Bi_2WO_6 and WO_3/Bi_2WO_6. (e) Schematic insertion of Bi atoms on the [WO_6] octahedral framework, WO_3/Bi_2WO_6 photogenerated carrier separation and the photocatalytic color change mechanism. Reproduced with permission.[26] Copyright 2023, Elsevier.

wavelength not only improves the solar photoelectricity utilization, but also generates more photogenerated electrons. The relationship between the band gap (E_g) and the excitation wavelength (λ) of semiconductor materials is shown as follows:

$$h\frac{c}{\lambda} \geq E_g, \tag{5}$$

where h is the Planck constant (6.63×10^{-34} J s) and c is the speed of light (2.998×10^8 m s^{-1} in vacuum).[54] Hence, reducing the band gap by modifying the material to redshift the excitation wavelength is one of the ways to effectively improve the photochromic properties of the material. In a recent study, Zhang *et al.* embedded photochromic WO_3 nanoparticles in a polyvinyl alcohol/polyacrylic acid two-component polymer (PVA/PAA).[13] The embedding of PVA/PAA resulted in a significant redshift in the absorption spectrum of the film, with the edge of the absorption band stretching from 400 nm to 550 nm, which increased its photosensitivity and sunlight availability. With homogeneous transparency and suitable density, the WO_3/PVA/PAA nanocomposite film is capable of plasmonic diffusion and electron transfer, which achieves an efficient photochromic reaction under broadband excitation (Fig. 3b and c). Tuning the band gap of WO_3 by elemental doping to improve its photochromic properties has been a common approach. Akoth Okwako *et al.* successfully synthesized Al–Pt co-doped WO_3 thin films on the surface of soda lime glass using a low-cost spin-coating and screen-printing method.[55] The band gaps of the Al-doped and Al–Pt co-doped WO_3 films were 1.88 eV and 1.95 eV, respectively, which were greatly reduced compared with the optical band gap of WO_3 (2.36 eV). Optical tests indicated that the optical transmittance of the device assembled from this photochromic thin film assembly decreased by 43.61% in 10 min, and more than 85% of the initial transmittance could be recovered by bleaching in the dark for 2 h.

Although the band gap can be modified to enhance light absorption, the complexation of photogenerated electrons and holes needs to be taken into account to obtain a better photochemical energy conversion efficiency. Suppressing photogenerated electron–hole pair composites, improving the carrier lifetime, increasing the number of photogenerated electrons in the system, and utilizing these carriers to initiate photochemical reactions lead to higher chemical reaction rates and photochemical energy–chemical energy conversion efficiencies. The construction of heterojunctions is one of the commonly used strategies to inhibit photogenerated electron–hole pair com-

plexation. Dong *et al.* synthesized WO_3/Bi_2WO_6 heterostructure nanoparticles with efficient sunlight-responsive photochromism by introducing Bi atoms into the $[WO_6]$ framework to form a $[Bi_2O_2]$ component (Fig. 3d).[26] The WO_3/Bi_2WO_6-type II heterostructure ensured efficient photoexcited electron transfer from Bi_2WO_6 to WO_3, and the abundant $[WO_6]$ units served as fast sites for trapping and consuming photogenerated electrons, effectively promoting the separation of photogenerated electrons and holes (Fig. 3e). In addition, compounding with organics or noble metals (Au, Ag, *etc.*) is also a common solution. Precious metals are deposited on the surface of semiconductors, forming a Schottky barrier at the interface between the two and facilitating the separation of photogenerated carriers.[56,57] As organics are electron donors and act as hole sacrificers to eliminate photogenerated holes in semiconductors, the compounding of photogenerated electrons and holes in the semiconductors themselves is prevented.[58,59] Si *et al.* introduced fluor-silane and designed a WO_3-based photochromic material with superamphiphobicity, low adhesion, heat and chemical resistance, as well as UV and abrasion resistance (Fig. 4a).[5] Fluor-silane acted as an electron donor to promote rapid electron transfer and proton insertion, which significantly improved the photochromic properties of WO_3. Subsequently, they verified the photochromic performance of the material and its surface antifouling and self-cleaning ability by UV repetitive writing erasure, as illustrated in Fig. 4b.

The photochromic behavior depends on the electronic energy band structure and charge transfer process, which are affected by the physical and chemical properties of the photochromic materials. G. Deonikar *et al.* introduced plasma ions (Cu and Al) and non-plasma ions (Zn and Sm) to modulate tungsten oxide hydride ($WO_3{\cdot}0.33H_2O$) nanostructures in order to enhance their reversible photochromic ability (Fig. 4c).[16] Based on the double insertion-extraction model of ions and electrons, they explained the effect of different metal ions on the photochromic mechanism of WO_3 (Fig. 4d). They found that the insertion of hot electrons generated by plasma

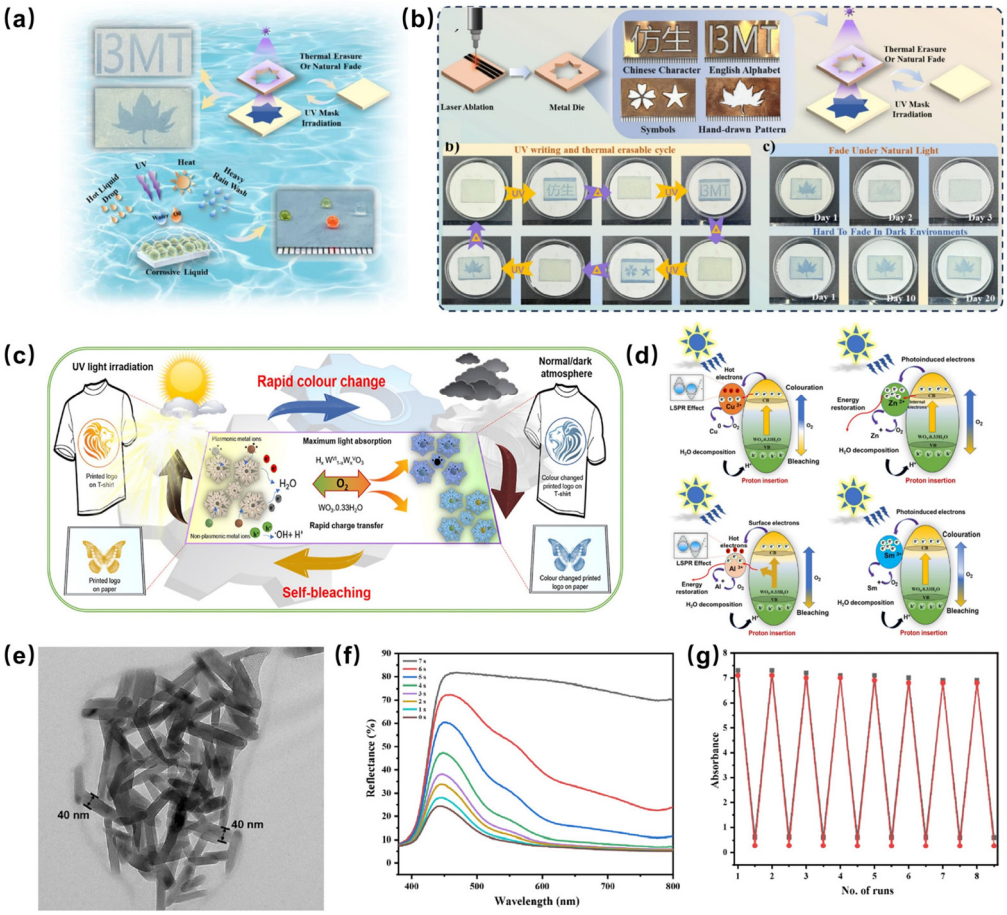

Fig. 4 (a) Schematic illustration of the F-WO_3/ZnO superamphiphobic powder surface adapting to harsh environmental conditions. (b) Process flow diagram for ultraviolet (UV) mask writing and thermal erasure. Reproduced with permission.[5] Copyright 2024, Elsevier. (c) Schematic demonstration of the photochromic process in $WO_3{\cdot}0.33H_2O$ hybrid nanostructures. (d) Schematic photochromic mechanism diagrams of different $WO_3{\cdot}0.33H_2O$ hybrid nanostructures. Reproduced with permission.[16] Copyright 2022, Elsevier. (e) HR-TEM pattern of the WO_3 nanofiber. (f) UV-Diffused reflectance spectra of the WO_3 nanofiber. (g) Number of photochromic reruns of the WO_3 nanofiber. Reproduced with permission.[27] Copyright 2022, Springer Nature.

metals (Cu and Al) into the $WO_3 \cdot 0.33H_2O$ nanostructures inhibited the complexation of photogenerated electrons and holes, enhanced light absorption, and improved the photochromic ability of the hybrid materials.

In addition to the structural design of WO_x photochromic materials, the modulation of morphology and size is also an important part to be considered in order to improve their photochromic properties, especially the light modulation ability and bleaching efficiency. Ejeromedoghene *et al.* reported a WO_3 nanofiber synthesized by non-electrostatic spinning under moderate conditions with particle diameters in the range of 200 nm (Fig. 4e).[27] This WO_3 fiber rapidly changed its visual color from white to blue with excellent reflectance (72%), reproducibility and stability after exposure to UV light for up to 7 s, as shown in Fig. 4f and g. Zhu *et al.* prepared extremely small-sized WO_3 quantum dots (WQDs) and WQDs-polyvinyl alcohol (PVA) transparent films by the casting method (Fig. 5a and b).[6] The WQDs are monodisperse near-spherical crystals with an average diameter of 1.2 nm.[60] Owing to the size effect of WQDs and the provision of protons by polyol, the composite films exhibited a fast light response (<60 s) and a large optical modulation amplitude (>90%) before and after coloration (Fig. 5c and d). However, their bleaching time was more than 8 h. Recently, Meng *et al.* reported a method for the *in situ* growth of WO_3 nanoparticles in PMMA matrix and obtained highly dispersed small-sized WO_3 nanoparticles in composite films simply and efficiently by utilizing the spatial confinement effect of PMMA chains (Fig. 5e).[18] This method allowed the preparation of photochromic films with high luminescence transparency (transmittance

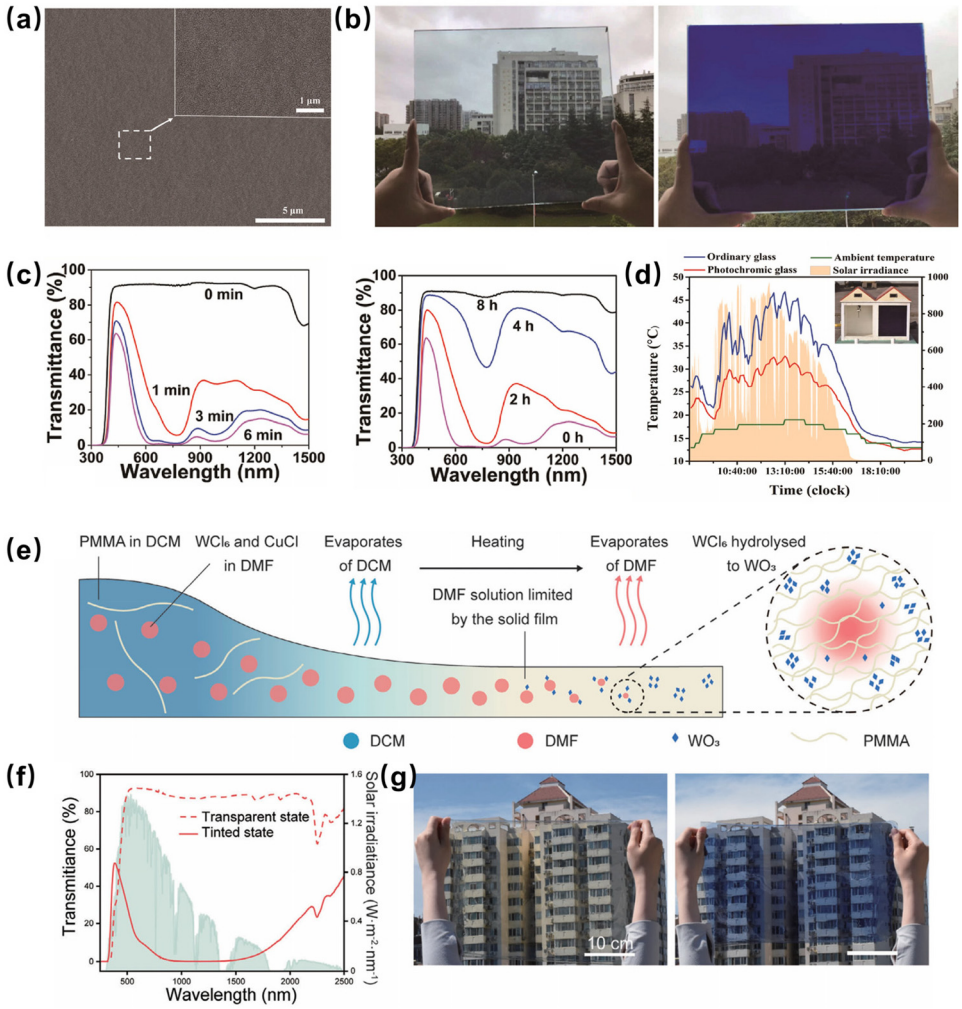

Fig. 5 (a) SEM image of the PVA WQD/PVA film. (b) Digital photographs of colored and bleached WQD-PVA films (25 cm × 30 cm). (c) Variation of the transmittance of the WQD-PVA film with UV irradiation time and its transmittance change at different times in the dark. (d) Real-time data of the outdoor experiment of the WQD-PVA film. Reproduced with permission.[6] Copyright 2022, Elsevier. (e) Schematic diagram of the preparation process of Cu-W-PC films. (f) Transmission spectra of Cu-W-PC films to standardized AM1.5 solar spectra (green shading) under coloring and bleaching conditions (6 h of outdoor sunlight). (g) Photographs of 30 × 40 cm^2 Cu-W-PC films prepared by the blade coating method in the bleached (left) and colored (right) states. Reproduced with permission.[18] Copyright 2023, John Wiley and Sons.

T_{lum} = 91%) and scalability (30 × 350 cm^2) at low cost. The high modulation of visible light (ΔT_{lum} = 73%) and solar heat (modulated solar transmittance ΔT_{sol} = 73% and modulated solar heat gain coefficient ΔSHGC = 0.5) by the films improved indoor daylight comfort and energy efficiency (Fig. 5f and g). Furthermore, they introduced Cu ions into this film to accelerate its bleaching process (20 min). This photochromic film, with its excellent light modulation capability, short bleaching time and ease of large-area preparation, offered an attractive strategy for achieving more energy-efficient buildings and carbon neutrality.

3.2 Electrochromism

Electrochromism is the phenomenon in which a material reversibly changes its color or optical properties (absorbance, transmittance, reflectance, *etc.*) through redox reactions in the presence of an applied voltage or current.[61–63] In 1961, the concept of "electrochromism" was first proposed by Platt.[64] Subsequently, Deb discovered the electrochromic phenomenon of WO_3 for the first time,[65] and proposed the electrochromic principle of the color-centered theory on the basis of this research, which became an important milestone in the history of the development of electrochromism.[66] As the most classic inorganic electrochromic material, WO_x has been widely used in the fields of infrared stealth,[67–69] flexible electronic devices,[70] and smart windows.[2,21,71,72]

Regarding the electrochromic mechanism of WO_3, the F-color core model and the dual ion implantation model are mainly discussed and accepted at present. The F-color center model was first proposed by Deb in 1973,[73] aiming to explain the electrochromic mechanism of amorphous WO_3 at that time. He suggested that amorphous WO_3 has an ionic crystal structure with oxygen vacancies in localized states, and that when a negative voltage is applied, electrons enter the oxygen vacancies and are trapped by them to form the F-color center, and the electrochromic film changes from colorless to blue. When a positive voltage is applied, the electrons are removed from the oxygen vacancies and the F-color center disappears, and the electrochromic film changes from blue to colorless. The dual ion implantation model, also known as the Faughnan model, is currently the most accepted mechanism model for electrochromism in the field since it explains not only the phenomenon of WO_3 electrochromism, but also other common electrochromic materials.[74] When a negative voltage is applied, the electrons enter into the interior of the material, and the cations enter at the same time and undergo valence transitions to produce the color change. When the opposite voltage is applied, the electrons and ions are simultaneously withdrawn, causing the color to return to its initial state.

There are mainly six performance parameters for evaluating electrochromic materials and devices. The first is the contrast ratio (CR), which reflects the degree of color changes of a material or device during the coloring or bleaching process, and is the basic index for evaluating the effect of color change. The second is optical density (OD), which describes the transmittance of the material or device at a constant wavelength, and is defined as:

$$OD = \lg\left(\frac{1}{T}\right), \quad (6)$$

where T is a constant wavelength at the transmittance. The third is coloration efficiency (CE), which refers to the unit area of power consumption caused by the absorbance of the degree of color change, defined as:

$$CE = \frac{\Delta A}{Q}, \quad (7)$$

where ΔA refers to the absorbance color change at a certain wavelength and Q refers to the power consumption per unit area. The fourth is the switching time (t), which refers to the time required to switch between the coloring and bleaching states. The switching time is related with many factors, such as the ionic conductivity of the electrolyte, the ionic diffusion rate, the thickness and morphology of the film layer, the magnitude of the applied voltage, *etc.* The fifth is the cycle life, which can be characterized by the number of cycles of repeating the coloring and bleaching processes.[74] In addition, the optical memory performance is one of the important indicators for evaluating electrochromic materials or devices. Optical memory performance, also called color stability, refers to the ability of optical properties (transmittance, reflectance, *etc.*) maintaining stability without external voltage.

Researchers have proposed various methods to enhance the performance of WO_x electrochromic materials, for instance, control of the structure and morphology, doping and compounding with other inorganic materials, and compounding with organics. Different synthesis approaches can yield WO_x with different nanostructures. Huang *et al.* found that the concentration of precursors plays an essential role in morphology control.[8] The morphology of WO_{3-x} ($0 < x < 1$) nanostructures gradually changed from nanowires (NWs), nanoclusters (NCs), to nanoflowers (NFs) with the increase of precursor concentration (Fig. 6a and b) and the color of the as-prepared WO_{3-x} nanostructure solutions gradually changed from light blue to dark blue, which indicated the increase of light absorption. It was also found that the lattice-stripe spacing of the WO_{3-x} nanostructures widened with increasing solution concentration. The weaker long-range ordering and lower crystallinity of WO_{3-x} NFs compared to WO_{3-x} NWs and WO_{3-x} NCs suggest that WO_{3-x} NFs are more conducive to the insertion/extraction of electrolyte ions in the electrochromic process. As shown in Fig. 6c, the WO_{3-x} NFs have the best optical modulation ability of 62.98% over WO_{3-x} NWs (52.06%) and WO_{3-x} NCs (61.01%) in the VIS and NIR regions, showing the importance of nanostructures. Fig. 6d shows the bright, cold and dark modulation modes of the WO_{3-x} NF electrochromic film, which demonstrates its potential application electrochromic smart windows. Du *et al.* prepared novel WO_{3-x} hydrate nanosheets by the template method, and the fabricated elec-

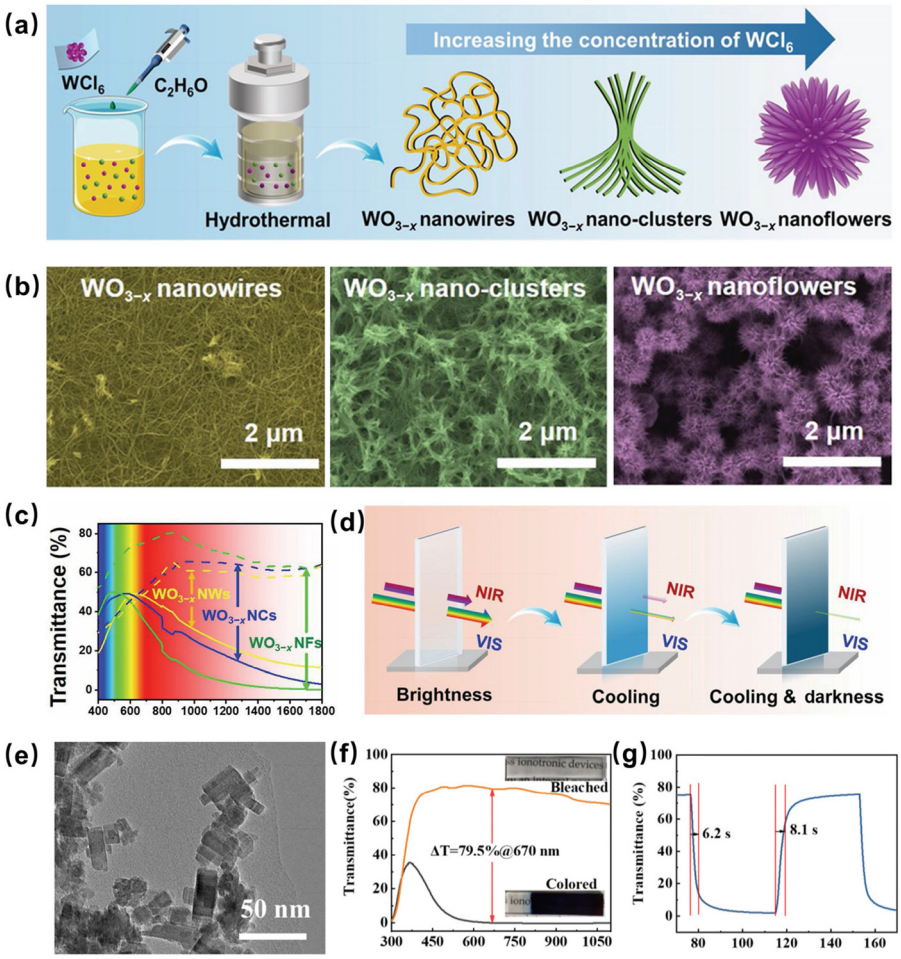

Fig. 6 (a) Synthesis process of WO_{3-x} with different structures and morphologies. (b) SEM images of WO_{3-x} NWs, WO_{3-x} NCs, and WO_{3-x} NFs. (c) Optical transmittance spectra of WO_{3-x} NWs, WO_{3-x} NCs and WO_{3-x} NFs in 1.0 M $LiClO_4$/PC electrolyte at −1.5 and 1.0 V. (d) Illustration of dual-band electrochromic smart windows in bright, cool, and dark modes. Reproduced with permission.[8] Copyright 2023, Springer Nature. (e) TEM images of the WO_{3-x} hydrate nanosheets. (f) Transmittance spectra in the bleached and colored states of the H-WO_{3-x} film. (g) *In situ* transmittance change curve between the colored state and the bleached state of the H-WO_{3-x} film in a cycle. Reproduced with permission.[11] Copyright 2022, Elsevier.

trochromic films exhibited excellent electrochemical and electrochromic properties (Fig. 6e and g).[11]

The crystalline phase structure of WO_x thin films has a significant effect on their electrochemical properties. Crystalline films prepared by conventional evaporation and magnetron sputtering have better cycling stability, yet they tend to be dense, which is not conducive to the diffusion of ions and will affect their coloring efficiency and response time.[75,76] It is generally recognized that amorphous films have a looser structure and more holes, which facilitates the diffusion of ions in them, and provides greater color contrast and speed of color change. Zhang *et al.* developed a fast-switching dual-band electrochromic smart window based on a single-component amorphous porous WO_3 (AP-WO_3) cathode (Fig. 7a and b).[3] The amorphous and porous structure of WO_3 not only significantly improves the ion transport, but also provides a large surface area for Li^+ adsorption, resulting in tunable surface plasmon resonance in the near-infrared range (Fig. 7c and d). As a result, the single-component AP-WO_3 films can independently and effectively modulate the near-infrared and visible transmittance through three different modes with high optical modulation and a fast switching speed, but their stability is slightly poor (Fig. 7e), which is also a common problem of amorphous WO_3 electrochromic films.[35,77,78] Pham *et al.* prepared WO_3 porous films on indium tin oxide (ITO) substrates using a simple three-pulse electrodeposition method.[79] These porous films outperformed the corresponding dense films formed by continuous electrodeposition in terms of long-term stability, with insignificant changes after 10 000 cycles. This research result will inspire more researchers to improve the preparation of electrodeposited films, reduce the preparation cost of electrochromic films, and promote the industrialization of electrochromic devices.

Compounding and doping of WO_x with other inorganic materials or elements is one of the most commonly used means to enhance its electrochromic properties. Most of the

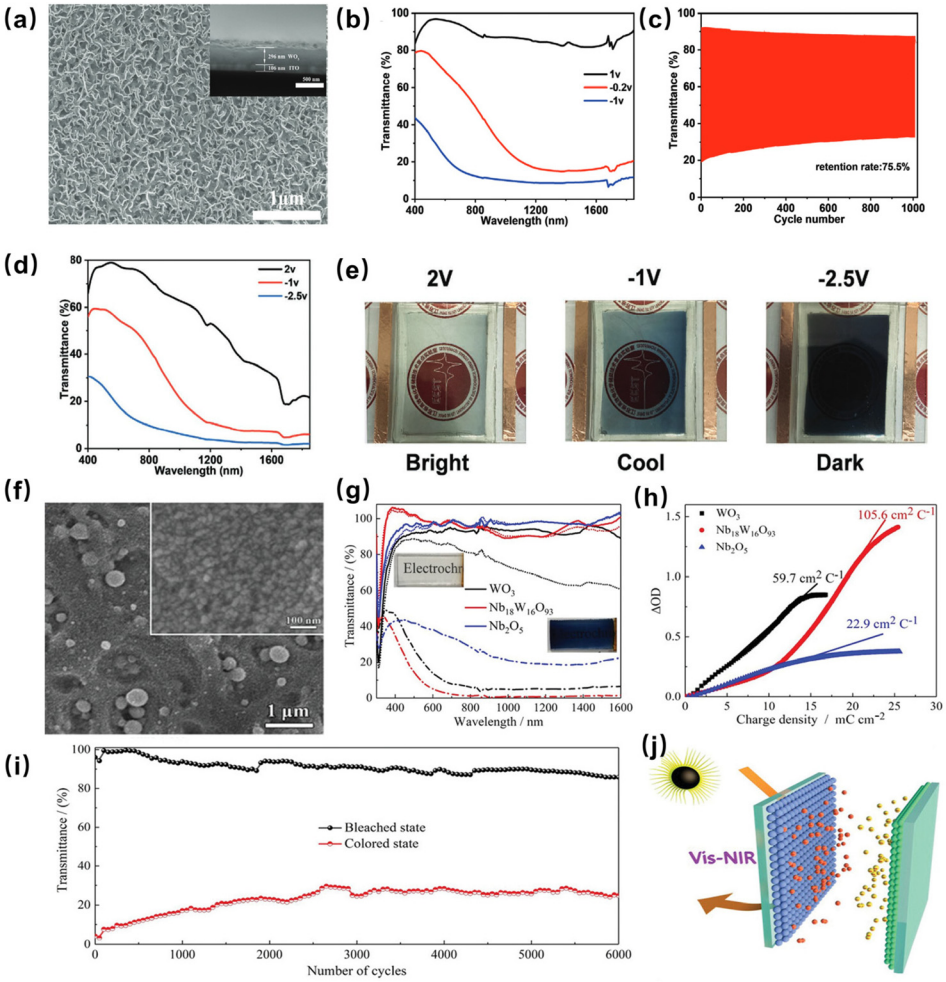

Fig. 7 (a) Surface and cross-section SEM images of AP-WO_3 thin films. (b) Transmittance spectra of AP-WO_3 thin films before and after coloring. (c) Cyclic stability test of AP-WO_3 thin films. (d) Transmittance spectra of the AP-WO_3 electrochromic device in bright, cold, and dark modes and (e) corresponding digital photographs. Reproduced with permission.[3] Copyright 2022, John Wiley and Sons. (f) SEM images of $Nb_{18}W_{16}O_{93}$ thin films. (g) Transmission spectra and (h) coloring efficiencies of WO_3, $Nb_{18}W_{16}O_{93}$, and Nb_2O_5 films in initial, colored, and bleached states. (i) Cycling stability test of the $Nb_{18}W_{16}O_{93}$ film. (j) Schematic diagram of the electrochromic energy storage device assembled with the $Nb_{18}W_{16}O_{93}$ film (green) as an electrochromic layer. Reproduced with permission.[15] Copyright 2022, John Wiley and Sons.

doping and compounding processes of WO_x were based on transition metals, especially focusing on transition metal oxides with electrochromic properties, such as Mo,[80] Ti,[81,82] *etc.* Cai *et al.* synthesized a $Nb_{18}W_{16}O_{93}$ nanomaterial with superstructural motifs and prepared homogeneous self-supported electrochromic thin films on transparent conductive substrates (Fig. 7f–i),[15] which showed large optical modulation (93% at 633 nm and 89% at 1200 nm), high color rendering efficiency (105.6 cm^2 C^{-1}), excellent multiplication capability and long-term electrochemical stability (6000 cycles). Based on this high-performance electrochromic film, they further assembled a multifunctional electrochromic energy storage device to realize the combination of dynamic dimming and energy storage applications (Fig. 7j). Such devices can not only manage solar thermal radiation entering a building and protect personal privacy, but also deposit electrical energy into it. The electrochromic films prepared in this work are low-cost and scalable, providing a new material option for electrochromic smart windows. Zhao *et al.* have constructed one-dimensional WO_3@PB arrays with porous core–shell structures.[7] As shown in Fig. 8a and b, the modification of WO_3 enables the film to have dual-band modulation capability at low voltage. Moreover, the porous one-dimensional structure of PB@WO_3 provides sufficient space for the lattice expansion of PB during the EC process, which improves the stability of PB (Fig. 8c). Owing to the formation of a heterostructure between PB and WO_3, the electron transfer is accelerated and the electronic interactions are enhanced, which further improves its electrochemical activity and stability.

Moreover, as a new doping means, oxygen vacancy doping significantly improves the electrochromic properties of WO_x, especially the modulation ability in the near-infrared band. Chen *et al.* reported a novel oxygen vacancy-modulated amorphous tungsten oxide (a-WO_{3-x}–O_v, $0 < x < 1$), as shown in

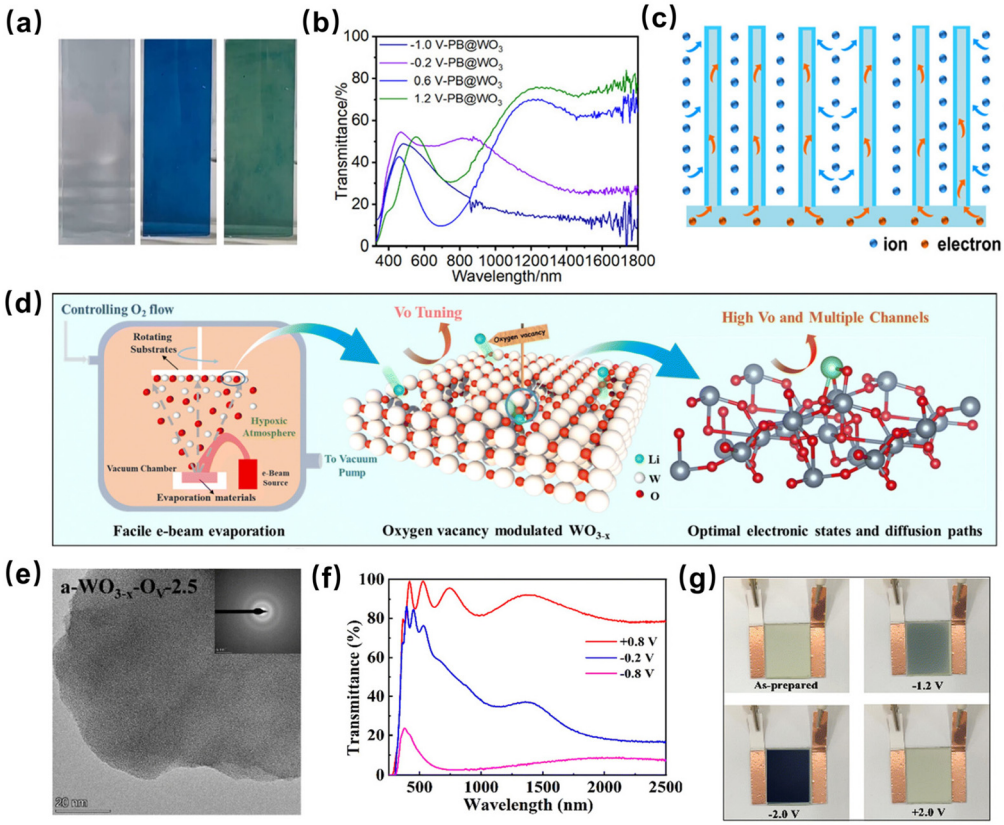

Fig. 8 (a) Digital photos of the PB@WO_3 film electrode at −0.2, 0.6, and 1.2 V. (b) UV–vis–NIR transmittance spectra of PB@WO_3 under different voltages of −1.0, −0.2, 0.6, and 1.2 V. (c) Schematic illustration of the EC mechanism in PB@WO_3. Reproduced with permission.[7] Copyright 2023, American Chemical Society. (d) Schematic illustration of the preparation and structure of oxygen vacancy-modulated a-WO_{3-x}–O_v thin films. (e) HRTEM image of the a-WO_{3-x}–O_v film. (f) Transmission spectrum of the a-WO_{3-x}–O_v thin film. (g) Corresponding digital photographs of the a-WO_{3-x}–O_v electrochromic device at different applied voltages. Reproduced with permission.[2] Copyright 2023, Royal Society of Chemistry.

Fig. 8d and e.[2] It was found that the introduction of oxygen vacancies not only enabled this film to modulate the near-infrared transmittance independently through the LSPR effect, but also provided more sites for ion diffusion and binding, which resulted in the optimum conductivity performance (Fig. 8f). They assembled these films into devices with effective energy storage performance and significant energy savings, which can greatly reduce the energy consumption of air conditioning and lighting in buildings, as shown in Fig. 8g. Additionally, as demonstrated in Fig. 9a, it can selectively control visible and NIR transmittance in three different modes: bright mode (+0.8 V, NIR and visible transparency), cold mode (0.2 V, visible transparency, mostly NIR opacity), and dark mode (0.8 V, NIR and visible opacity). Among the non-metallic element doping N[83] and phosphorus[84] doped WO_3 films have also been reported. It is worth mentioning that due to the superior electrochromic properties of WO_x itself, the doping of W atoms into various electrochromic oxides also leads to a better enhancement in their properties.[85] Wang *et al.* fabricated single tungsten atom (W)-modified hydrangea-like porous V_2O_5 nanoflowers (HLP-W/V_2O_5) with a high loading content of atomic W (13.7 wt%) using a low-temperature solvothermal method (Fig. 9b and c).[17] The ion diffusion and electronic conductivity of HLP-W/V_2O_5 were greatly improved with the assistance of W atom modification. Below 1.2 V, HLP-W/V_2O_5 exhibited three reversible color transformations (yellow, blue, and brown) and excellent cycling stability (10 000 cycles without significant decay), as demonstrated in Fig. 9d–f.

As a typical representative of inorganic electrochromic materials, WO_x possesses excellent chemical stability, but it also has the drawbacks of singular color change and a slow response speed, thus compositing with organic materials is a reliable method to realize its fast response and multiple color change. Nguyen *et al.* reported an electrochromic hybrid film based on polyaniline and WO_3, which achieved multiple color changes (green, blue, violet and dark blue) in a single film and has ultra-short switching times (1.5 s for each of the coloring and bleaching processes) and cycle lifetimes (Fig. 9g).[28] Xue *et al.* constructed an electrolyte-free, integrated electrochromic device using WO_3 sols doped with carbon nanodots (CDs).[86] Unlike conventional WO_3 that exhibit color transitions between transparent and blue, the device enabled reversible color changes between yellow and green due to the intrinsic color of the carbon dots. Their study provided a new idea for the composite of WO_x and organic materials.

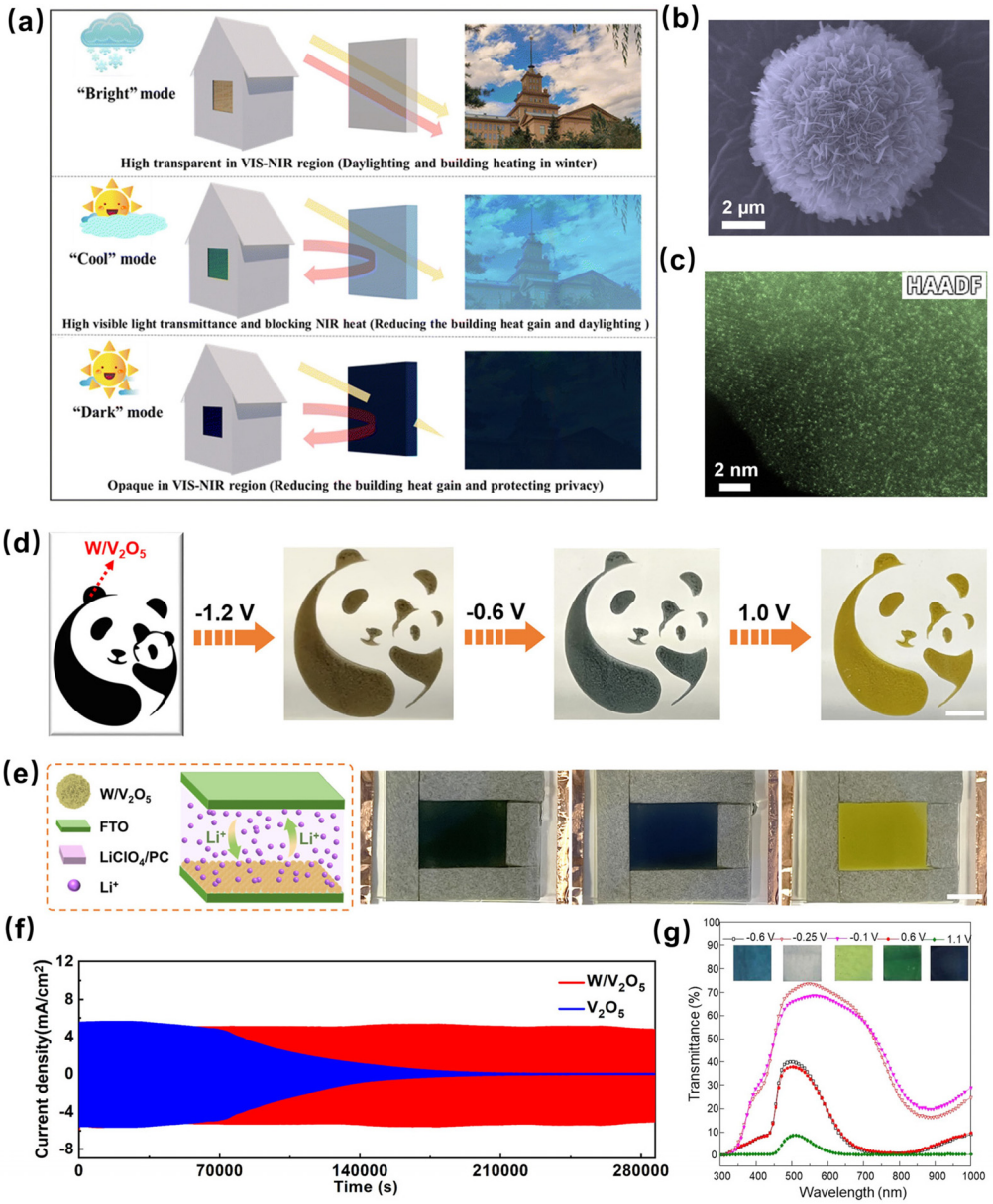

Fig. 9 (a) Application scenarios of the a-WO_{3-x}–O_v electrochromic device in bright, cool, and dark operation modes. Reproduced with permission.[2] Copyright 2023, Royal Society of Chemistry. (b) SEM images of HLP-W/V_2O_5. (c) AC HAADF-STEM image of HLP-W/V_2O_5. (d) Prototype of the panda fabricated based on HLP-W/V_2O_5 and photographs at different colored states. (e) Structural schematic diagram of the solid EC device and photographs of the solid EC device at different color states. (f) Cycling stability of HLP-V_2O_5 and HLP-W/V_2O_5 with multi-potential steps between −0.6 and 1 V for 79.4 h. Reproduced with permission.[17] Copyright 2023, Elsevier. (g) Transmittance of PANI-WO_3 thin films at different applied voltages. Reproduced with permission.[28] Copyright 2021, Elsevier.

3.3 Gasochromism

The gasochromism effect refers to the interaction of a material with a target gas, which causes changes in the optical properties of the material, such as transparency, reflectivity, and color changes. Typically, the material returns to its initial state after isolation of the target gas, and the process is reversible.[87] The target gas may be different for different materials. As for WO_3, the target gas is H_2. Therefore, the gasochromism of WO_3 can also be called hydrochromic response.

Since the gasochromism of WO_3 was studied later than its electrochromism, there are relatively limited studies on its gasochromic mechanism. In this review, we choose the commonly used double-injection model to explain the H_2 gasochromic mechanism of WO_3. Compared with electrochromism, the coloration process of WO_3 under an H_2 atmosphere is much more complicated. During the coloration process, H_2 molecules are adsorbed on the catalyst surface and dissociate into H atoms, which further diffuse along the surface and finally inject into the WO_3 in the form of H^+ and electrons,

which is known as the so-called double injection. There is only one charge transfer reaction in the double injection process, where an electron from the H atom is transferred into WO_3, reducing the W^{6+} ion to W^{5+}. In the bleaching process, O_2 adsorbed on the surface dissociates and transfers to form chemically active O atoms or O^{2-}, which attracts and combines with the H atoms to form an H_2O molecule, and then the H_2O is desorbed, thus causing discoloration of the film.[88] The above coloring and bleaching processes can be described by eqn (8) and (9):

$$WO_3 + \frac{x}{2}H_2 \rightarrow H_xWO_3 \quad (8)$$

$$H_xWO_3 + \frac{x}{4}O_2 \rightarrow WO_3 + \frac{x}{2}H_2O\uparrow \quad (9)$$

It can be analyzed from the WO_3 hydrochromic mechanism that the discoloration rate of WO_3 is mainly related to the adsorption of H_2, the diffusion of H atoms in WO_3, and the chemical reaction between H atoms and WO_3. On the other hand, the adsorption and diffusion of H_2 are closely related to the distribution of the catalyst as well as the composition and structure of the material. Except for the effect of temperature, it is difficult to accelerate the chemical reaction between H atoms and WO_3 by other methods. Hence, it can be designed from the morphological structure and composition in order to improve the hydrochromic performance of WO_3.

Foroushan *et al.* prepared three WO_3 nanofiber meshes by electrostatic spinning.[89] WO_3 nanofiber meshes had good sensitivity to hydrogen gas (in argon) down to 2% at room temperature. Upon exposure to hydrogen, the almost colorless nanofibers turned blue in less than 2 min. Liu *et al.* synthesized sub-stabilized hexagonal WO_3 with three typical morphologies using a hydrothermal method, which exhibited excellent hydrochromic properties.[90] Moreover, they pointed out that the correlation between the morphology and the hydrochromic properties was mainly attributed to the growth difference of the preferred crystalline surface of WO_3. The evaluation of the morphology of WO_3 nanowires, microspheres and nanorods exhibited a decrease in the aspect ratio, which corresponds to the microscopically preferred growth orientation changing from (002) to (100). Increasing the exposure ratio of oxygen ions on the *c*-axis by morphological modulation can improve the injection process of WO_3 and promote the coloring process. This is helpful to deepen the understanding of the morphology effect of WO_3 in the H_2 gas chromatography process and to provide theoretical guidance for the preparation of highly sensitive WO_3 gas chromatography materials. A detailed study of the hydrochromic properties of WO_3 at different operating temperatures, solvation conditions (low, medium, high) and doping concentrations has been carried out by Nisha *et al.* and the effect of precious metal (Pt, Pd) doping on the hydrochromic properties has been discussed.[91] The results show that the hydrochromic response increases significantly with increasing working temperature, and the Pt-doped samples exhibit better hydrochromic response than the Pd-doped samples. A low detection limit of 0.01% was observed for the samples at temperatures between 50 °C and 100 °C, and they did not show any cross-sensitivity to other gases. It is a positive contribution to the development of hydrogen sensors based on WO_3. More and further research is needed to be put into the gasochromism of WO_3, which would be a significant advancement forward in gas sensing.

4. Summary and outlook

This review focuses on the functional mechanisms, performance indexes, properties, and applications of WO_x in photochromism, electrochromism and gasochromism. WO_x materials have been widely investigated in recent years due to their tunnel-like structure, sub-stoichiometric properties, and polycrystalline phase. However, there are still many challenges for WO_x, such as the structural design, stability improvement, large-scale and low-cost preparation, *etc.* Much effort should be made for the development of WO_x in intelligent chromogenic technology. It is crucial to improve the long-term stability of WO_x materials to realize their practical applications. There is an urgent need to combine nanostructure design and multiple synthesis methods to construct a series of WO_x materials with long-term stable recycling. Since WO_x-based photothermal management devices typically have a multilayer structure and interactions between the layers, an appropriate device structural design is critical. In the case of electrochromic devices, the selection of different substrates, transparent conductive layers, and electrolytes has a significant impact on the performance and sustainability of the devices. In addition, large-scale preparation of high-performance WO_x films at a reasonable cost is crucial. Currently, electrodeposition, electrostatic spinning, sol–gel, *etc.* are the main approaches for the preparation of WO_x films. However, their cost and scale are not suitable for practical production. Hence, it is essential to improve the traditional preparation techniques and investigate new preparation techniques to promote its industrial development and application.

Data availability

No primary research results, software or code have been included and no new data were generated or analysed as part of this review.

Conflicts of interest

There are no conflicts to declare.

Acknowledgements

This work was supported by the Tsinghua-Toyota Joint Research Fund, the National Key Research and Development Program of China (Grant No. 2020YFC2201103 and

2020YFA0210702), the Jiangsu Specially Appointed Professor program and the Postgraduate Research & Practice Innovation Program of Jiangsu Province (KYCX24_1486).

References

1 R. Pardo, M. Zayat and D. Levy, *Chem. Soc. Rev.*, 2011, **40**, 672–687.
2 M. Chen, X. Zhang, D. Yan, J. Deng, W. Sun, Z. Li, Y. Xiao, Z. Ding, J. Zhao and Y. Li, *Mater. Horiz.*, 2023, **10**, 2191–2203.
3 S. Zhang, Y. Peng, J. Zhao, Z. Fan, B. Ding, J. Y. Lee, X. Zhang and Y. Xuan, *Adv. Opt. Mater.*, 2023, **11**, 2202115.
4 P. A. Shinde and S. C. Jun, *ChemSusChem*, 2020, **13**, 11–38.
5 W. Si, S. Wang, Z. Yu, X. Dai, M. Guo and Z. Guo, *Chem. Eng. J.*, 2024, **492**, 152232.
6 Y. Zhu, Y. Yao, Z. Chen, Z. Zhang, P. Zhang, Z. Cheng and Y. Gao, *Sol. Energy Mater. Sol. Cells*, 2022, **239**, 111664.
7 S. Zhao, B. Wang, Y. Huang, Y. Zhang, X. Wu, Q. Jiang, D. Gao, F. Wang, R. Li, Y. Li, Y. Zhao, J. Li and R. Zhang, *ACS Appl. Nano Mater.*, 2023, **6**, 15021–15028.
8 Y. Huang, B. Wang, P. Lyu, S. Zhao, X. Wu, S. Zhang, R. Li, Q. Jiang, F. Wang, Y. Zhao and R. Zhang, *Nano Res.*, 2023, **16**, 12165–12172.
9 K. O. Brinkmann, P. Wang, F. Lang, W. Li, X. Guo, F. Zimmermann, S. Olthof, D. Neher, Y. Hou, M. Stolterfoht, T. Wang, A. B. Djurišić and T. Riedl, *Nat. Rev. Mater.*, 2024, **9**, 202–217.
10 Y. Li, X. Ru, M. Yang, Y. Zheng, S. Yin, C. Hong, F. Peng, M. Qu, C. Xue, J. Lu, L. Fang, C. Su, D. Chen, J. Xu, C. Yan, Z. Li, X. Xu and Z. Shao, *Nature*, 2024, **626**, 105–110.
11 J. Du, Z. Zhang, C. Yue, Z. Nie, H. Tan, Z. Tang, N. Li, L. Xu and J. Xu, *Mater. Today Chem.*, 2022, **26**, 101089.
12 S. Bandi and A. K. Srivastav, *J. Mater. Sci.*, 2021, **56**, 6615–6644.
13 M. Zhang, J. Miao, H. Liu, S. Fu, X. Li, Y. Tao, X. Qi and X. Zhang, *J. Mater. Chem. C*, 2022, **10**, 7690–7698.
14 X. Qiu, Y. Wang and M. Shao, *Joule*, 2024, **8**, 881–882.
15 G. Cai, R. Zhu, S. Liu, J. Wang, C. Wei, K. J. Griffith, Y. Jia and P. S. Lee, *Adv. Energy Mater.*, 2022, **12**, 2103106.
16 V. G. Deonikar and H. Kim, *Mater. Today Chem.*, 2022, **26**, 101080.
17 B. Wang, Y. Huang, Y. Han, S. Zhao, W. Ding, W. Zhang, R. Li, X. Wu, Q. Jiang, Y. Li, D. Gao, Y. Zhao, F. Wang, H. Jiang and R. Zhang, *Cell Rep. Phys. Sci.*, 2023, **4**, 101408.
18 W. Meng, A. J. J. Kragt, Y. Gao, E. Brembilla, X. Hu, J. S. van der Burgt, A. P. H. J. Schenning, T. Klein, G. Zhou, E. R. van den Ham, L. Tan, L. Li, J. Wang and L. Jiang, *Adv. Mater.*, 2024, **36**, 2304910.
19 A. Dhakshinamoorthy, Z. Li, S. Yang and H. Garcia, *Chem. Soc. Rev.*, 2024, **53**, 3002–3035.
20 S. Li, G. Du, M. Pan, X. Wang, X. Dong, T. Huang, D. Hu, T. Ren, X. Li, H. Chen and X. Mai, *Adv. Compos. Hybrid Mater.*, 2024, **7**, 15.
21 Z. Shao, A. Huang, C. Cao, X. Ji, W. Hu, H. Luo, J. Bell, P. Jin, R. Yang and X. Cao, *Nat. Sustain.*, 2024, **7**, 796–803.
22 F.-X. Zhao, M.-H. Wang, Z.-Y. Huang, M.-H. Zhu, C. Chen, Q.-H. Pan, B. Yu, Y.-T. Wang, X. Guo, Y.-J. Qian, L.-W. Zhang, X.-J. Qiu, S.-Z. Sheng, Z. He, J.-L. Wang and S.-H. Yu, *Adv. Mater.*, 2024, **36**, 2408192.
23 J. Zhao, S. Zhang, S. Chang, C. Li, C. Fang, X. Xia, L. Shen, J. Yang Lee, C. Cao, X. Zhang and Y. Xuan, *Chem. Eng. J.*, 2024, **480**, 148010.
24 Y. Deng, Y. Yang, Y. Xiao, X. Zeng, H.-L. Xie, R. Lan, L. Zhang and H. Yang, *Adv. Mater.*, 2024, **36**, 2401869.
25 Y. Li, P. Sun, J. Chen, X. Zha, X. Tang, Z. Chen, Y. Zhang, S. Cong, F. Geng and Z. Zhao, *Adv. Mater.*, 2023, **35**, 2300116.
26 X. Dong, Y. Shao, X. Ren, Z. Li, K. Li, Y. Tong, X. Liu and Y. Lu, *Appl. Surf. Sci.*, 2023, **636**, 157783.
27 O. Ejeromedoghene, X. Zuo, S. O. Ogungbesan, O. Oderinde, F. Yao, S. Adewuyi and G. Fu, *J. Mater. Sci.: Mater. Electron.*, 2022, **33**, 7371–7379.
28 T. V. Nguyen, H. H. Do, T. Q. Trung, Q. V. Le, T. P. Nguyen, S. H. Hong, H. W. Jang, S. H. Ahn and S. Y. Kim, *J. Alloys Compd.*, 2021, **882**, 160718.
29 Y. Wang, H. Yin, X. Zhao, Y. Qu, A. Zheng, H. Zhou, W. Fang and J. Li, *Appl. Catal., B*, 2024, **341**, 123266.
30 Y. Zhang, W. Zheng, H. Wu, R. Zhu, Y. Wang, M. Wang, T. Ma, C. Cheng, Z. Zeng and S. Li, *SusMat*, 2024, **4**, 106–115.
31 K. Wang, L. Luo, C. Wang and J. Tang, *Chin. J. Catal.*, 2023, **46**, 103–112.
32 Y.-G. Lee, G. Yoo, Y.-R. Jo, H.-R. An, B.-R. Koo and G.-H. An, *Adv. Energy Mater.*, 2023, **13**, 2300630.
33 M. Zhang, K. Liu, X. Zhang, B. Wang, X. Xu, X. Du, C. Yang and K. Zhang, *J. Adv. Ceram.*, 2022, **11**, 1860–1872.
34 P. Roussel, P. Labbe and D. Groult, *Acta Crystallogr., Sect. B: Struct. Sci.*, 2000, **56**, 377–391.
35 P. Liu, B. Wang, C. Wang, L. Ma, W. Zhang, E. Hopmann, L. Liu, A. Y. Elezzabi and H. Li, *Adv. Funct. Mater.*, 2024, **34**, 2400760.
36 W. Cheng, J. He, K. E. Dettelbach, N. J. J. Johnson, R. S. Sherbo and C. P. Berlinguette, *Chem*, 2018, **4**, 821–832.
37 S. Cong, F. Geng and Z. Zhao, *Adv. Mater.*, 2016, **28**, 10518–10528.
38 A. Al Mohammad and M. Gillet, *Thin Solid Films*, 2002, **408**, 302–309.
39 H. Watanabe, K. Fujikata, Y. Oaki and H. Imai, *Chem. Commun.*, 2013, **49**, 8477–8479.
40 Z. Li, J. Zi, X. Luan, Y. Zhong, M. Qu, Y. Wang and Z. Lian, *Adv. Funct. Mater.*, 2023, **33**, 2303069.
41 C. Hu, J. Yin, S. Xun, L. Zhu, H. Li, M. He, P. Wu, H. Li and W. Zhu, *Appl. Catal., B*, 2024, **355**, 124155.
42 J. A. Delgado-Notario, D. López-Díaz, D. McCloskey and J. M. Caridad, *Adv. Funct. Mater.*, 2024, **34**, 2401599.
43 X. Liu, L. Yang, M. Huang, Q. Li, L. Zhao, Y. Sang, X. Zhang, Z. Zhao, H. Liu and W. Zhou, *Appl. Catal., B*, 2022, **319**, 121887.

44 Y. Huang, K. Dai, J. Zhang and G. Dawson, *Chin. J. Catal.*, 2022, **43**, 2539–2547.
45 H. Gu, Y. Zhao, M. Tan, S. Zhang, P. Wen, H. Cheng, Y. Yan and D. Hu, *Mater. Lett.*, 2022, **321**, 132407.
46 M. Zhang, C. Yang, Z. Zhang, W. Tian, B. Hui, J. Zhang and K. Zhang, *Adv. Colloid Interface Sci.*, 2022, **300**, 102596.
47 Z. Zhang, J. Liang, K. Liu, W. Tian, X. Liang, K. Zhao and K. Zhang, *ACS Sens.*, 2024, **9**, 4196–4206.
48 Z. Zou, Z. Zhao, Z. Zhang, W. Tian, C. Yang, X. Jin and K. Zhang, *Anal. Chem.*, 2023, **95**, 2110–2118.
49 X. Li, M. Liu, J. Shao, H. Sun, Q. Zhang, D. Peng and F. Liu, *Adv. Funct. Mater.*, 2024, **34**, 2402603.
50 P. Li, Y. Wang, X. He, Y. Cui, J. Ouyang, J. Ouyang, Z. He, J. Hu, X. Liu, H. Wei, Y. Wang, X. Lu, Q. Ji, X. Cai, L. Liu, C. Hou, N. Zhou, S. Pan, X. Wang, H. Zhou, C.-W. Qiu, Y.-Q. Lu and G. Tao, *Light: Sci. Appl.*, 2024, **13**, 48.
51 T. Ma, B. Li, S. Tian, J. Qian, L. Zhou, Q. Liu, B. Liu, X. Zhao and G. Sankar, *Chem. Eng. J.*, 2023, **468**, 143587.
52 X. Dong, Y. Lu, Z. Wu, X. Liu and Y. Tong, *Chem. Eng. J.*, 2023, **477**, 147064.
53 W. Meng, A. J. J. Kragt, X. Hu, J. S. van der Burgt, A. P. H. J. Schenning, Y. Yue, G. Zhou, L. Li, P. Wei, W. Zhao, Y. Li, J. Wang and L. Jiang, *Adv. Funct. Mater.*, 2024, **34**, 2402494.
54 Ş. Neaţu, V. I. Pârvulescu, G. Epure, E. Preda, V. Şomoghi, A. Damin, S. Bordiga and A. Zecchina, *Phys. Chem. Chem. Phys.*, 2008, **10**, 6562–6570.
55 J. Akoth Okwako, S. H. Song, S. Park, H. V. Tran, B. O. Aduda, S. Waita, Y.-S. Hong, S. Hong and C.-H. Han, *Electrochem. Commun.*, 2024, **165**, 107762.
56 S. Yamazaki and K. Isoyama, *J. Phys. Chem. B*, 2022, **126**, 6520–6528.
57 X. Yan, W. Zhong, S. Qu, Z. Li and L. Shang, *J. Colloid Interface Sci.*, 2023, **646**, 855–862.
58 M. S. Kim, H. K. Lee, J. H. Yoon, H. M. Kim, Y. S. Kim and J. P. Kim, *Colloids Surf., A*, 2024, **694**, 134083.
59 Q. Zhang, R. Wang, Y. Lu, Y. Wu, J. Yuan and J. Liu, *ACS Appl. Mater. Interfaces*, 2021, **13**, 4220–4229.
60 Y. Yao, Q. Zhao, W. Wei, Z. Chen, Y. Zhu, P. Zhang, Z. Zhang and Y. Gao, *Nano Energy*, 2020, **68**, 104350.
61 B. Deng, Y. Zhu, X. Wang, J. Zhu, M. Liu, M. Liu, Y. He, C. Zhu, C. Zhang and H. Meng, *Adv. Mater.*, 2023, **35**, 2302685.
62 S. Kandpal, T. Ghosh, C. Rani, A. Chaudhary, J. Park, P. S. Lee and R. Kumar, *ACS Energy Lett.*, 2023, **8**, 1870–1886.
63 P. Lei, J. Wang, Y. Gao, C. Hu, S. Zhang, X. Tong, Z. Wang, Y. Gao and G. Cai, *Nano-Micro Lett.*, 2023, **15**, 34.
64 J. R. Platt, *J. Chem. Phys.*, 1961, **34**, 862–863.
65 S. K. Deb, *Appl. Opt.*, 1969, **8**(Suppl 1), 192–195.
66 S. K. Deb, *Philos. Mag.*, 1973, **27**, 801–822.
67 K. Chein Sheng Ly, H. Zhang, X. Liu, D. Tang, J. Xu, X. Fu, H. Zhou and T. Fan, *J. Am. Ceram. Soc.*, 2021, **104**, 2143–2157.
68 M. Li, W. Jiang, Y. Lin, C. Huang, P. Hao, W. Wang, L. Yang, Y. Wang and D. Wang, *J. Mater. Chem. C*, 2024, **12**, 5420–5430.
69 T. Ghosh, S. Kandpal, L. Bansal, B. Sahu, D. K. Rath, C. Rani and R. Kumar, *Adv. Eng. Mater.*, 2024, **26**, 2400013.
70 L. Brändler, L. Niklaus, M. Schott and P. Löbmann, *Adv. Mater. Technol.*, 2023, **8**, 2201903.
71 M. Chen, X. Zhang, W. Sun, Y. Xiao, H. Zhang, J. Deng, Z. Li, D. Yan, J. Zhao and Y. Li, *Nano Energy*, 2024, **123**, 109352.
72 X. Tong, J. Wang, P. Zhang, P. Lei, Y. Gao, R. Ren, S. Zhang, R. Zhu and G. Cai, *Chem. Eng. J.*, 2023, **470**, 144130.
73 S. K. Deb, *Sol. Energy Mater. Sol. Cells*, 2008, **92**, 245–258.
74 Y. Huang, B. Wang, F. Chen, Y. Han, W. Zhang, X. Wu, R. Li, Q. Jiang, X. Jia and R. Zhang, *Adv. Opt. Mater.*, 2022, **10**, 2101783.
75 K. Pandurangarao, N. Purnachand and V. Ravi Kumar, *Opt. Mater.*, 2020, **101**, 109791.
76 T.-S. Yang, Z.-R. Lin and M.-S. Wong, *Appl. Surf. Sci.*, 2005, **252**, 2029–2037.
77 Z. Han, M. Tong, C. Zhang, X. Guo, Y. Chen, W. Chen, H. Zhong, J. Wan, S. Cai, Y. Ma, C. Wang, S. Cong and Z. Wang, *Sol. Energy Mater. Sol. Cells*, 2024, **273**, 112939.
78 Z. Li, Z. Liu, L. Zhao, Y. Chen, J. Li and W. Yan, *J. Alloys Compd.*, 2023, **930**, 167405.
79 N. S. Pham, L. T. Nguyen, H. T. Nguyen, V. Q. Nguyen, T. B. T. Nguyen, C. D. Tran, B. N. Nguyen and A. Q. K. Nguyen, *Ceram. Int.*, 2023, **49**, 33413–33417.
80 P. J. Morankar, R. U. Amate, A. M. Teli, S. A. Beknalkar, G. T. Chavan, N. A. Ahir and C.-W. Jeon, *J. Energy Storage*, 2024, **84**, 110978.
81 Q. Meng, S. Cao, J. Guo, Q. Wang, K. Wang, T. Yang, R. Zeng, J. Zhao and B. Zou, *J. Energy Chem.*, 2023, **77**, 137–143.
82 M. Hassan, A. Ghaffar, G. Lou, Z. Miao, Z. Peng and K. Celebi, *Adv. Funct. Mater.*, 2024, **34**, 2310535.
83 G. Atak, İ. Bayrak Pehlivan, J. Montero, D. Primetzhofer, C. G. Granqvist and G. A. Niklasson, *Mater. Today: Proc.*, 2020, **33**, 2434–2439.
84 C. O. Avellaneda and L. O. S. Bulhões, *J. Solid State Electrochem.*, 2003, **7**, 183–186.
85 G. Gao, X. Tao, Y. He, Z. Li, J. Zhuang, L. He, Y. Li, Y. Wang, D. Sun and A. Xie, *Appl. Surf. Sci.*, 2023, **640**, 158346.
86 Z. Xue, Q. Li, M. Yu, Y. Lv, H. Sun, Y. Zhang and D. Wang, *Phys. Lett. A*, 2020, **384**, 126822.
87 J. Domaradzki, D. Kaczmarek, D. Wojcieszak and M. Mazur, *Sens. Actuators, B*, 2014, **201**, 420–425.
88 S. Lee, H. Cheong, P. Liu, D. Smith, C. E. Tracy, A. Mascanrenhas, J. R. Pitts and S. K. Deb, *J. Appl. Phys.*, 2000, **88**, 3076–3078.
89 F. Tavakoli Foroushani, H. Tavanai, M. Ranjbar and H. Bahrami, *Sens. Actuators, B*, 2018, **268**, 319–327.
90 D. Liu, Z. Geng, A. Han, P. Yu, K. Zhang, H. Liu and Y. Liu, *Int. J. Hydrogen Energy*, 2024, **60**, 20–27.
91 Nisha and P. K. Basu, *IEEE Sens. J.*, 2023, **23**, 1854–1866.
92 O. Glember and H. Saurr, *Z. Anorg. Chem.*, 1943, **252**(3–4), 144–159.